Analysis of elastic scattering of $^{16}O+^{28}Si$ and $^{12}C+^{24}Mg$ by a new optical potential

G. S. Mallick,[1] S. K. Agarwalla,[2] B. Sahu,[2] and C. S. Shastry[3]
[1]*Department of Physics, Khallikote College, Berhampur 760 001, India*
[2]*Department of Physics, North Orissa University, Baripada 757 003, India*
[3]*Department of Physics, Amrita Vishwa Vidyapeetham, Coimbatore 641 105, India*
(Received 30 May 2005; revised manuscript received 6 March 2006; published 9 May 2006)

We construct a new phenomenological nucleus-nucleus optical potential based on the interesting potential developed by Ginocchio that has the versatility to control the surface and volume regions of the potential. Using this potential with suitable energy dependence of some of the parameters, we are able to fit remarkably well experimental results of the differential scattering cross section for the $^{16}O+^{28}Si$ system in the center-of-mass energy $E_{c.m.}$ range from 18.67 to 90.681 MeV and the excitation function in the $E_{c.m.}$ range from 13.0 to 52.0 MeV. We also fit equally well the exhaustive experimental differential scattering data available for the $^{12}C+^{24}Mg$ system in the $E_{c.m.}$ range from 10.67 to 16.0 MeV. The new optical potential used has significantly fewer parameters. The results are interpreted in terms of wave mechanical aspects leading to superposition of partial waves undergoing different phase shifts generated by an optical potential characterized by volume and surface parts.

DOI: 10.1103/PhysRevC.73.054606 PACS number(s): 24.10.Ht, 25.70.Bc

I. INTRODUCTION

The phenomenological optical model with an attractive complex nuclear potential is widely applied for the analysis of the measured elastic scattering cross section, fusion cross section, and inelastic scattering cross section in heavy-ion collisions (HIC). In this article, we deal with the $^{16}O+^{28}Si$ and $^{12}C+^{24}Mg$ collisions over a wide energy range. These are interesting HIC systems because experimental results of angular variation of the differential cross section $d\sigma/d\sigma_R$ of the $^{16}O+^{28}Si$ and $^{12}C+^{24}Mg$ systems are marked by high oscillation at energies around and much above the Coulomb barrier. Mermaz *et al.* [1] have measured and studied the $^{16}O+^{28}Si$ system and are unable to produce oscillations at low energies by their optical potential. Kobos and Satchler [2] have calculated the measured data of Mermaz for the $^{16}O+^{28}Si$ system with the folding potential supplemented in the surface with a double peaked attractive correction. The data at the higher energy ($E_{c.m.} \geqslant 20.83$ MeV) were well fitted but at low energy ($E_{c.m.} \leqslant 20.12$ MeV) the calculations did not produce the observed oscillations. Similarly, energy- and parity-dependent optical potentials [3] were successful in explaining the back angle oscillations at higher energies in the $^{16}O+^{28}Si$ system but could not reproduce the observed oscillations at energies near the Coulomb barrier. Shastry and Parija [4] have studied the $^{16}O+^{28}Si$ system at incident laboratory energy $E_{Lab} = 55.0$ MeV with particular reference to orbiting phenomena generated by the comparatively flat barrier. Recently I. Boztosun [5] has explained elastic scattering differential cross section for all energies by taking a very deep Woods-Saxon-type form factor for real and imaginary parts of nuclear potential. To fit the data, they have added an extra term to the potential given by the first derivative of the Woods-Saxon form factor. Further, they have considered an imaginary part that consists of a deep volume part near the origin and deep surface part near the surface. Thus, the whole conventional phenomenological nuclear optical potential is modified rampantly to fit the data at lower energies.

Sciani *et al.* [6] have measured elastic scattering differential cross sections of the $^{12}C+^{24}Mg$ system at 15 energies near the Coulomb barrier between $E_{c.m.} = 10.67$ and 16.00 MeV. Angular distributions of this system present strong oscillations at almost all energies, with the exception of the lowest energies, and they could not be fitted simultaneously by previously used optical potential families [7–13] with simple energy dependence and normal absorption. Therefore, Sciani *et al.* [6] have analyzed the data with Q-value-dependent potential parameters in an ad hoc fashion. Boztosun *et al.* [14] have also explained the results of $d\sigma/d\sigma_R$ of the $^{12}C+^{24}Mg$ system using standard coupled-channel calculations with addition of an extra coupling potential that is the first derivative of Woods-Saxon shape.

In this article, we analyze elastic scattering of the $^{16}O+^{28}Si$ and $^{12}C+^{24}Mg$ systems with the specific objective of analyzing the data over a wide energy range, from $E_{c.m.} = 18.67$ to 90.681 MeV in the case of the $^{16}O+^{28}Si$ system and $E_{c.m.} = 10.67$ to 16.00 MeV in the case of the $^{12}C+^{24}Mg$ system. In these energy ranges, the behavior of $d\sigma/d\sigma_R$ shows wide angular variation, indicating different type of processes dominating at different energies. To analyze this in a comprehensive manner, we use a nuclear optical potential constructed using the versatile Ginocchio potential [15,16]. It may be noted that recently we have used such a potential for the detailed successful study of elastic scattering, resonances, and fusion of the $^{12}C+^{12}C$ system [16]. And this has prompted us to use this potential in the optical model analysis described in this article. In particular, we have found that by our construction it is possible to address volume and surface parts of the potential distinctly, which has been found to be necessary by Boztosun to produce required amplitude and phase of oscillations in the

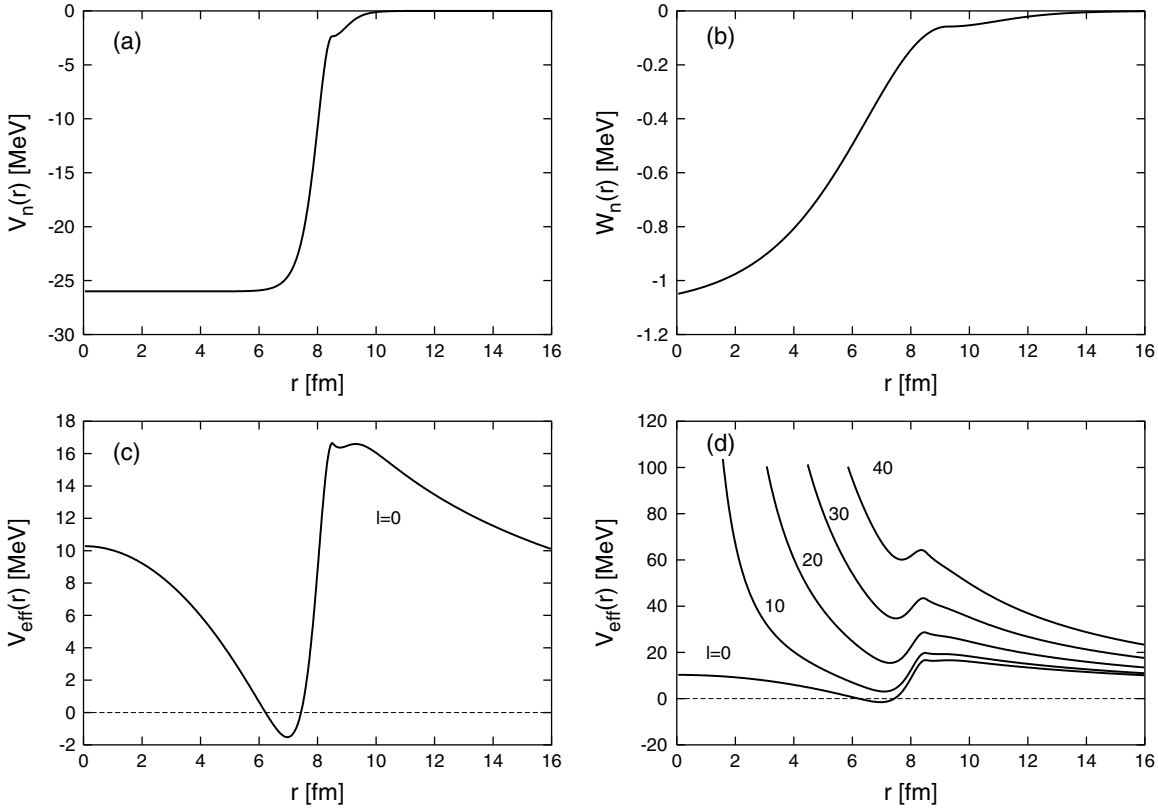

FIG. 1. (a) Plot of $V_n(r)$ expressed by Eq. (2) at $E_{\text{c.m.}} = 19.03$ MeV. Values of the parameters for $V_n(r)$ are: $R_0 = 8.5$ fm, $B_0 = 26$ MeV, $B_1 = 0.6$, $B_2 = 0.53$, and $V_B = 2.35$ MeV. (b) Plot of $W_n(r)$ expressed by Eq. (3) at $E_{\text{c.m.}} = 19.03$ MeV. Values of the parameters for $W_n(r)$ are $R_{0W} = 9.25$ fm, $W_0 = 1.1$, $W_1 = 0.5$, $W_2 = 0.18$, and $V_{BW} = 0.058$ MeV. (c) Plot of real part of $V_{\text{eff}}(r)$ expressed by Eq. (1) at $E_{\text{c.m.}} = 19.03$ MeV for $\ell = 0$. (d) Plot of real part of $V_{\text{eff}}(r)$ expressed by Eq. (1) at $E_{\text{c.m.}} = 19.03$ MeV for $\ell = 0$, 10, 20, 30, and 40.

differential scattering cross section for both the HIC systems studied in this article.

In Sec. II, we present the formulation of the optical potential based on our earlier work [16]. Section III is devoted to the application of our new optical potential to analyze the angular variation of differential scattering cross sections and the corresponding excitation function for the ^{16}O+^{28}Si system. In Sec. IV, we describe the results of calculations for the ^{12}C+^{24}Mg system. Section V contains discussions and conclusions.

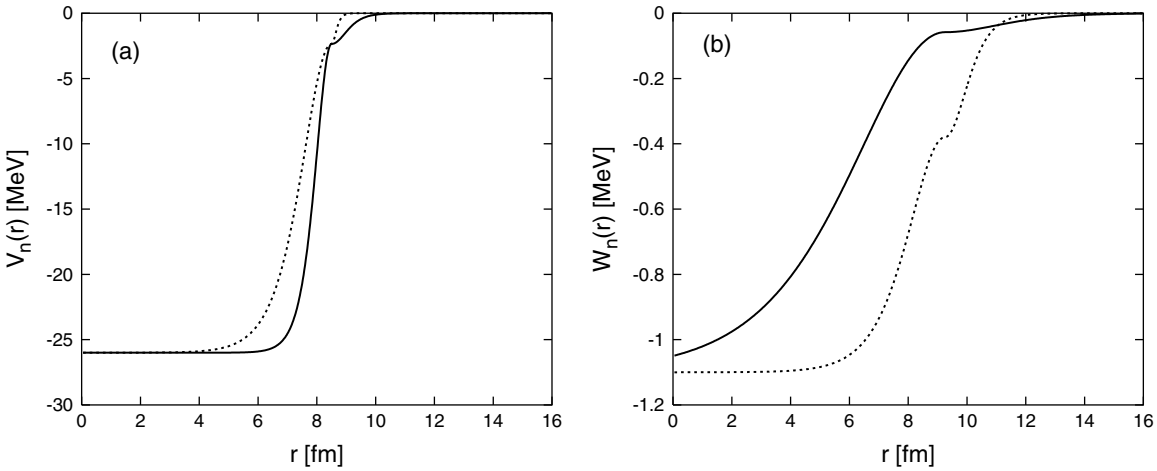

FIG. 2. (a) Plot of $V_n(r)$ expressed by Eq. (2). The dashed line indicates the potential $V_n(r)$ with parameters $B_1 = 2.05$ and $B_2 = 0.05$ for energy $E_{\text{c.m.}} = 26.20$ MeV and the solid line indicates the same with parameters $B_1 = 0.6$ and $B_2 = 0.53$ for $E_{\text{c.m.}} = 19.03$ MeV. (b) Plot of $W_n(r)$ expressed by Eq. (3). The dashed line indicates the potential $W_n(r)$ with parameter $V_{BW} = 0.38$ MeV for $E_{\text{c.m.}} = 26.20$ MeV and the solid line indicates the same with parameter $V_{BW} = 0.058$ MeV for $E_{\text{c.m.}} = 19.03$ MeV.

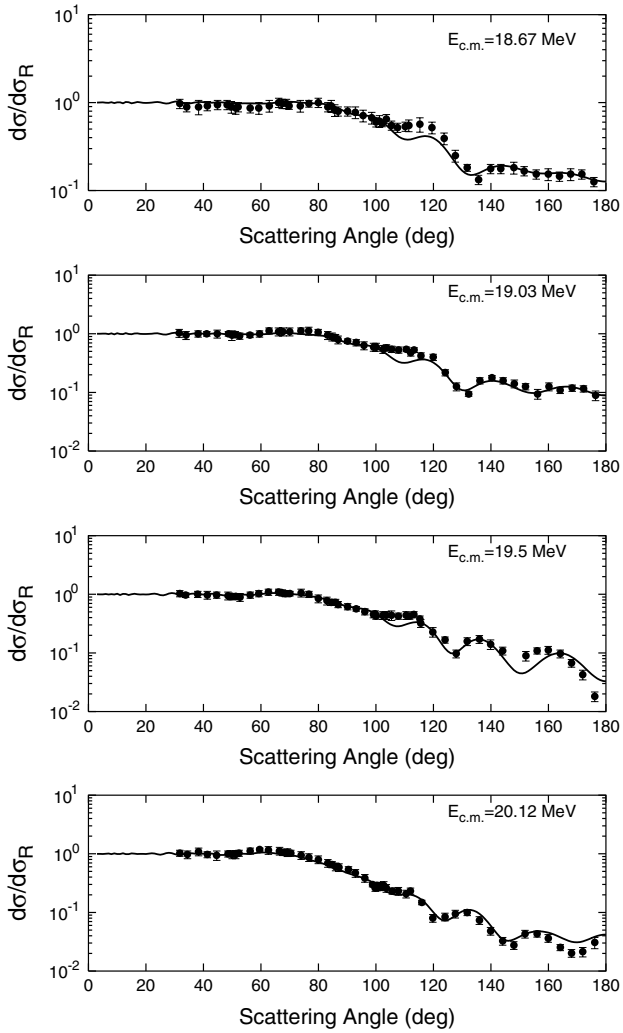

FIG. 3. Angular variation of elastic scattering cross sections of $^{16}O+^{28}Si$. Calculated results are shown by solid curves. The experimental data points are obtained from Ref. [2].

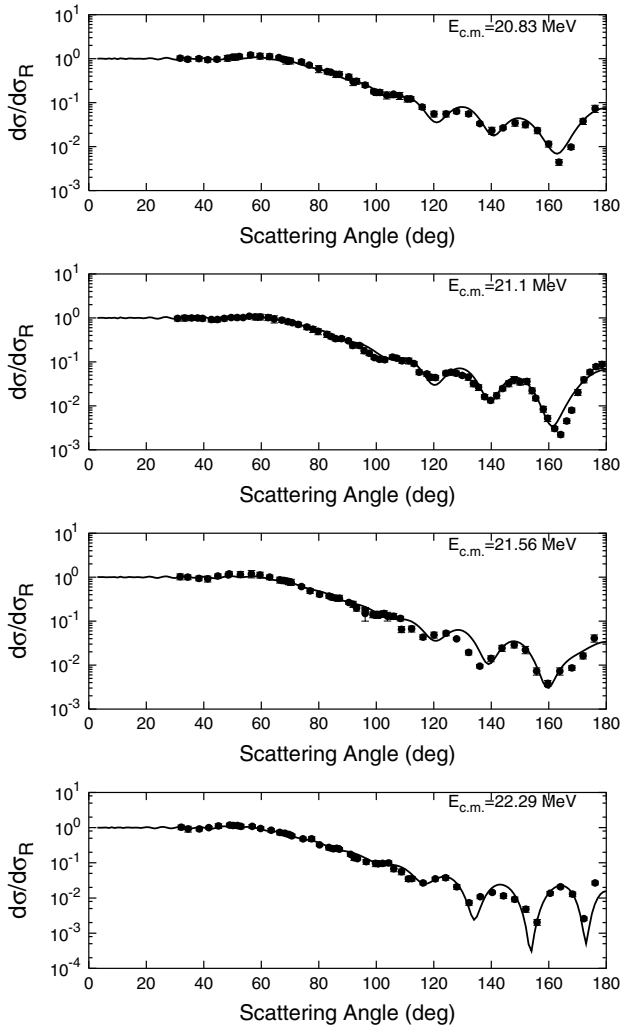

FIG. 4. Angular variation of elastic scattering cross sections of $^{16}O+^{28}Si$. Calculated results are shown by solid curves. The experimental data points are obtained from Ref. [2].

II. FORMULATION

In the optical model calculations, the effective nucleus-nucleus potential governing the nucleus-nucleus collision is

$$V_{\text{eff}}(r) = V_N(r) + V_C(r) + \frac{\ell(\ell+1)\hbar^2}{2\mu r^2}, \tag{1}$$

where μ is the reduced mass and $V_N(r) = V_n(r) + iW_n(r)$ is the nuclear optical potential. In our calculations, the real part of the nuclear optical potential has the form [16]

$$V_n(r) = \begin{cases} -\frac{V_B}{B_1}\left[B_0 + (B_1 - B_0)\left(1 - y_1^2\right)\right], & \text{if } 0 < r < R_0 \\ -\frac{V_B}{B_2}\left[B_2\left(1 - y_2^2\right)\right], & \text{if } r \geqslant R_0, \end{cases} \tag{2}$$

where $y_n = \tanh \rho_n$, $\rho_n = (r - R_0)b_n$ with the slope parameter $b_n = \sqrt{2mV_B}/\hbar^2 B_n$, $n = 1, 2.R_0$ is a radial distance in the surface region close to the radial position of the effective s-wave barrier potential generated by Eq. (1). B_0 controls the depth of the potential at the origin $r = 0.V_B$, indicating the depth of the potential at $r = R_0$ in MeV, controls the slope parameter b_n. Further, b_n is controlled by the parameter B_n on either side of R_0. It is seen that small value of B_n, making b_n large, allows the potential to change sharply.

Unlike monotonically decreasing behavior of the nuclear potential in the case of standard Woods-Saxon form, in our construction, the nuclear potential $V_n(r)$ shows a slight nontrivial behavior near $r = R_0$. At this point, the two parts of the potentials corresponding to interior (volume) region and outer (surface) region with different rate of decrease of amplitudes are connected. To ensure analytic continuation without any irregularities at $r = R_0$, we make sure that in addition to the potentials being same at $r = R_0$, the respective derivatives respect to r give same value (zero in this case) at this point of joining. The necessity of such a consideration for the nuclear potential stems from the fact that in the surface region around $r = R_0$, the two bombarding nuclei touch each other and one visualizes the occurrence of processes, namely resonance phenomena belonging to the formation of composite binuclear system, effects of frictional forces, and transfer of one or cluster of nucleons from the target to the projectile

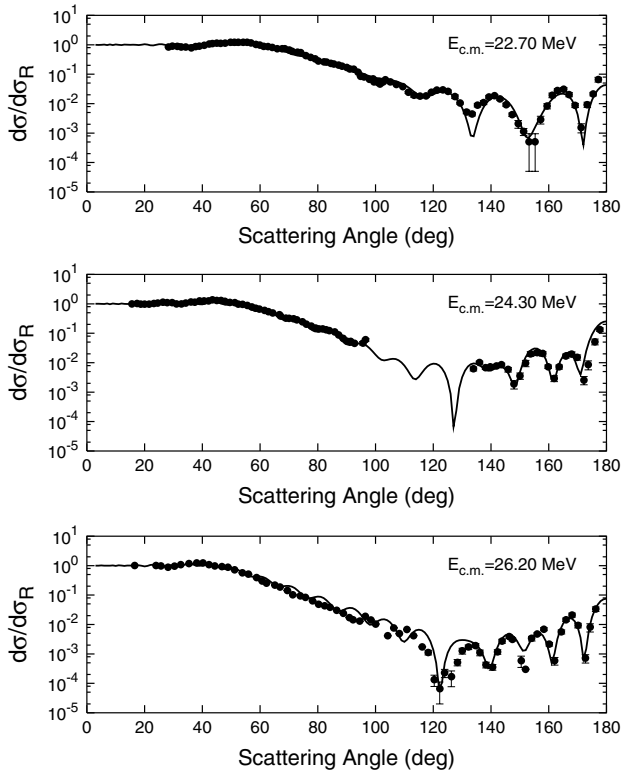

FIG. 5. Angular variation of elastic scattering cross sections of ^{16}O+^{28}Si. Calculated results are shown by solid curves. The experimental data points are obtained from Ref. [2].

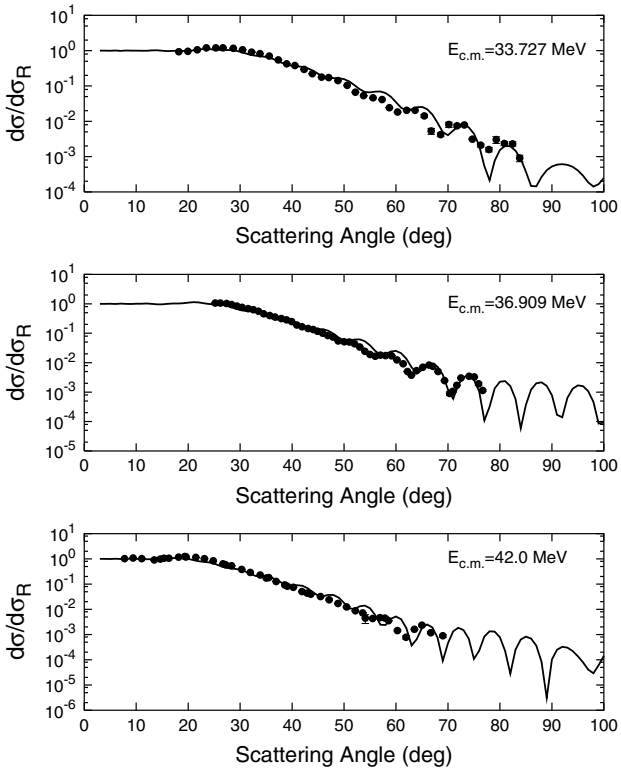

FIG. 7. Angular variation of elastic scattering cross sections of ^{16}O+^{28}Si. Calculated results are shown by solid curves. The experimental data points are obtained from Refs. [9–22].

and/or vice versa in this configuration. The microscopic double folding procedure that predicts the shape of the nuclear potential in the Woods-Saxon form usually does not include the features stated above. Hence, one has to look for some other form of nuclear potential that incorporates the effects stated above either by basic formulation or by phenomenology. For example, within the framework of phenomenological

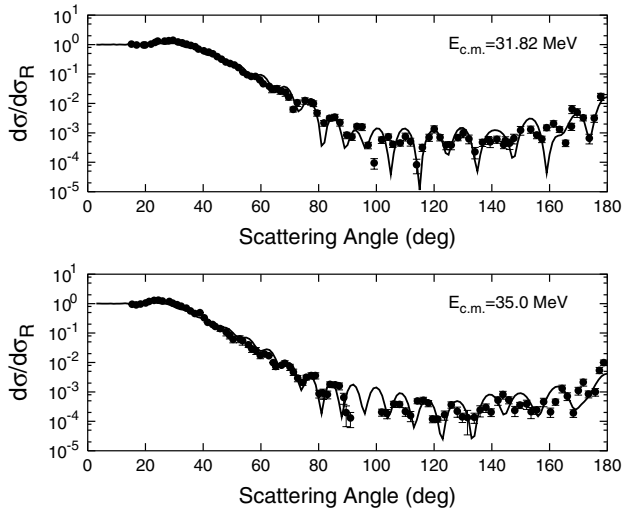

FIG. 6. Angular variation of elastic scattering cross sections of ^{16}O+^{28}Si. Calculated results are shown by solid curves. The experimental data points are obtained from Ref. [2].

consideration, to account for the transfer of nucleons, the exchange potentials for the nuclear part are written sometimes under the form $V_n = V_1 + (-1)^\ell V_2$, where V_1 is a standard Woods-Saxon potential and V_2 has the form $V_2 = -Ne^{\beta r}/r$. This modification ultimately leads to a change in the shape of the nuclear potential given by standard Woods-Saxon potential only. In our present work, we incorporate this expected change in the shape of the nuclear potential by the expression given by Eq. (2), which can be seen in the plot of $V_n(r)$ as a function of r in Fig. 1(a). We, then, seek the validity of this new form of nuclear potential by obtaining perfect fittings of the measured data of differential scattering cross sections over a wide range of energy in the cases of two well-known systems, namely ^{16}O+^{28}Si and ^{12}C+^{24}Mg.

From the quantum mechanical point of view, we may mention that the potential considered here does not generate any irregularities namely discontinuity or different values of slopes at $r = R_0$ in the variation of amplitude of wave function as a function of radial distance at a given energy. This nature of smooth continuation of wave function justifies the physical nature of the nuclear potential adopted in this analysis of HIC.

The imaginary part of the potential has the same form as that of $V_n(r)$ but with different strength. This is expressed as

$$W_n(r) = \begin{cases} -\frac{V_{BW}}{W_1}\left[W_0 + (W_1 - W_0)\left(1 - y_{1w}^2\right)\right], & \text{if } 0 < r < R_{0W} \\ -\frac{V_{BW}}{W_2}\left[W_2\left(1 - y_{2w}^2\right)\right], & \text{if } r \geqslant R_{0W}. \end{cases} \quad (3)$$

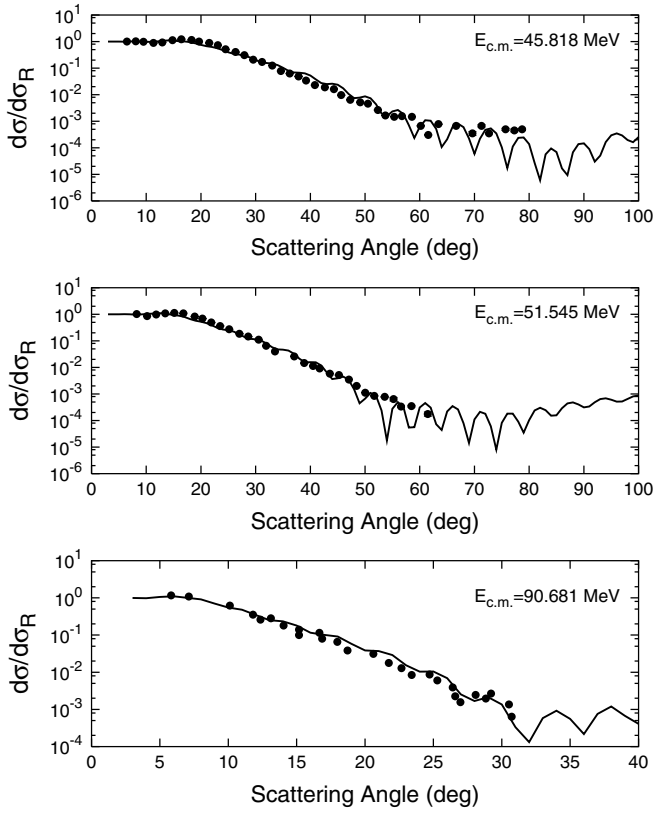

FIG. 8. Angular variation of elastic scattering cross sections of $^{16}O+^{28}Si$. Calculated results are shown by solid curves. The experimental data points are obtained from Refs. [9–22].

This is plotted in Fig. 1(b). The Coulomb potential between colliding nuclei is taken to be

$$V_C(r) = \begin{cases} \frac{Z_P Z_T e^2}{2{R_C}^3}\left(3{R_C}^2 - r^2\right), & \text{if } r < R_C \\ \frac{Z_P Z_T e^2}{r}, & \text{if } r > R_C, \end{cases} \quad (4)$$

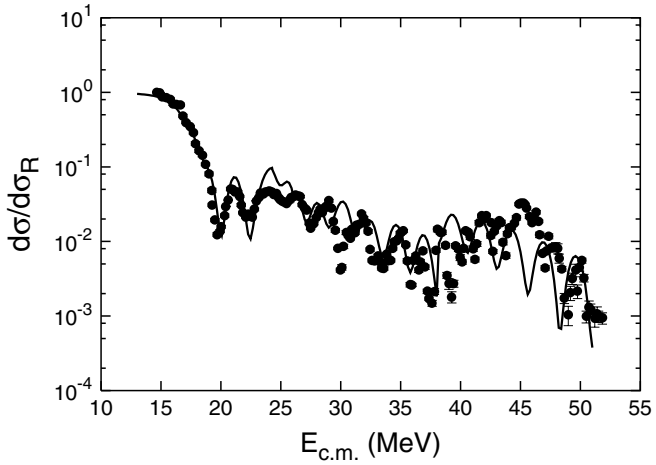

FIG. 9. Comparison of the calculated 180° elastic scattering excitation function with measured experimental data. The theoretical calculation is averaged over last 5°. Calculated results are shown by solid curves. The experimental data points are obtained from Ref. [2].

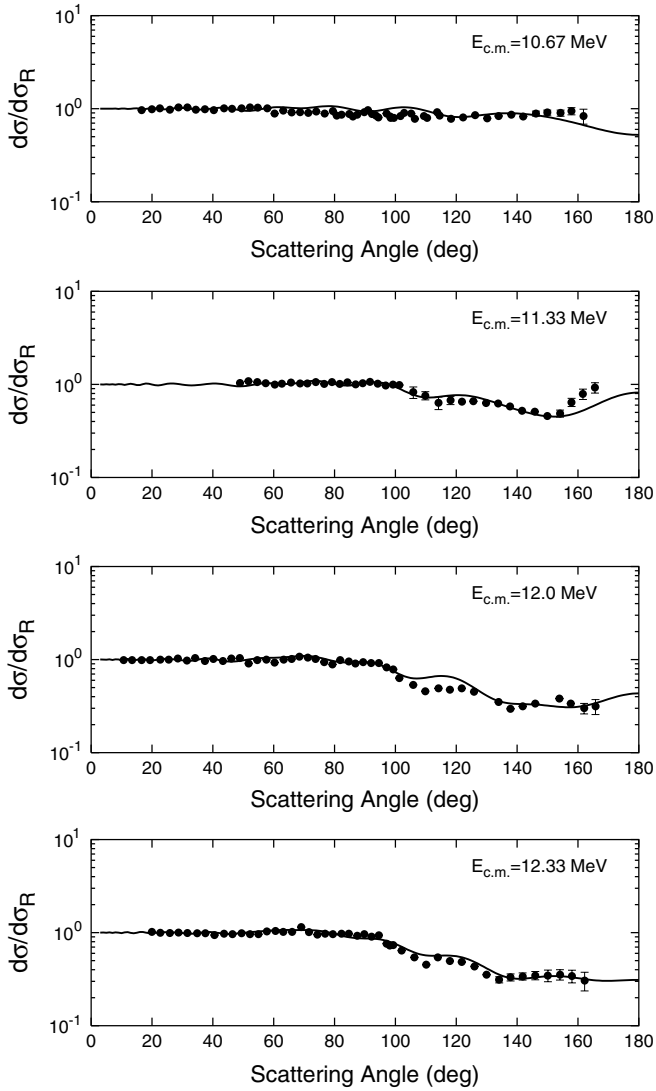

FIG. 10. Angular variation of elastic scattering cross section of $^{12}C+^{24}Mg$. The calculated results are shown by solid curve. The experimental values are shown by solid dots obtained from Ref. [6].

where $R_C = r_C({A_P}^{1/3} + {A_T}^{1/3})$. A_P and A_T are the mass number of projectile and target, respectively. Z_P and Z_T are the corresponding proton numbers. We have set the Coulomb radius parameter $r_C = 1.2$ fm in our calculation. The real part of $V_{\text{eff}}(r)$ given by Eq. (1) is shown in Fig. 1(c) for $\ell = 0$ and in Fig. 1(d) for different ℓs. Using this potential, we solve the Schroedinger equation to obtain the scattering amplitudes $f(\theta)$ and nuclear amplitude $f_n(\theta)$. The total scattering amplitude $f(\theta)$ can be expressed as

$$f(\theta) = f_C(\theta) + f_n(\theta) \quad (5)$$

$$= f_C(\theta) + \frac{1}{2ik}\sum_\ell (2\ell+1)e^{2i\sigma_\ell} P_\ell(\cos\theta)(e^{2i\bar{\delta}_\ell} - 1), \quad (6)$$

where $f_C(\theta)$ is the Coulomb amplitude, σ_ℓ is the Coulomb phase shift, and $\bar{\delta}_\ell$ is the nuclear phase shift. The differential

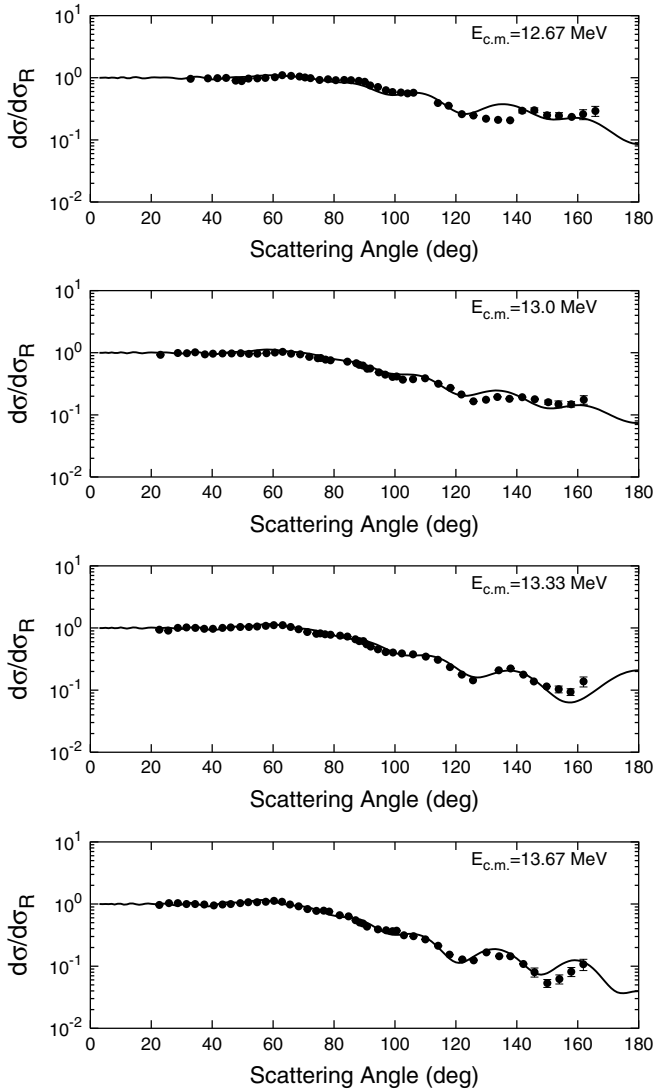

FIG. 11. Angular variation of elastic scattering cross section of $^{12}C+^{24}Mg$. The calculated results are shown by solid curve. The experimental values are shown by solid dots obtained from Ref. [6].

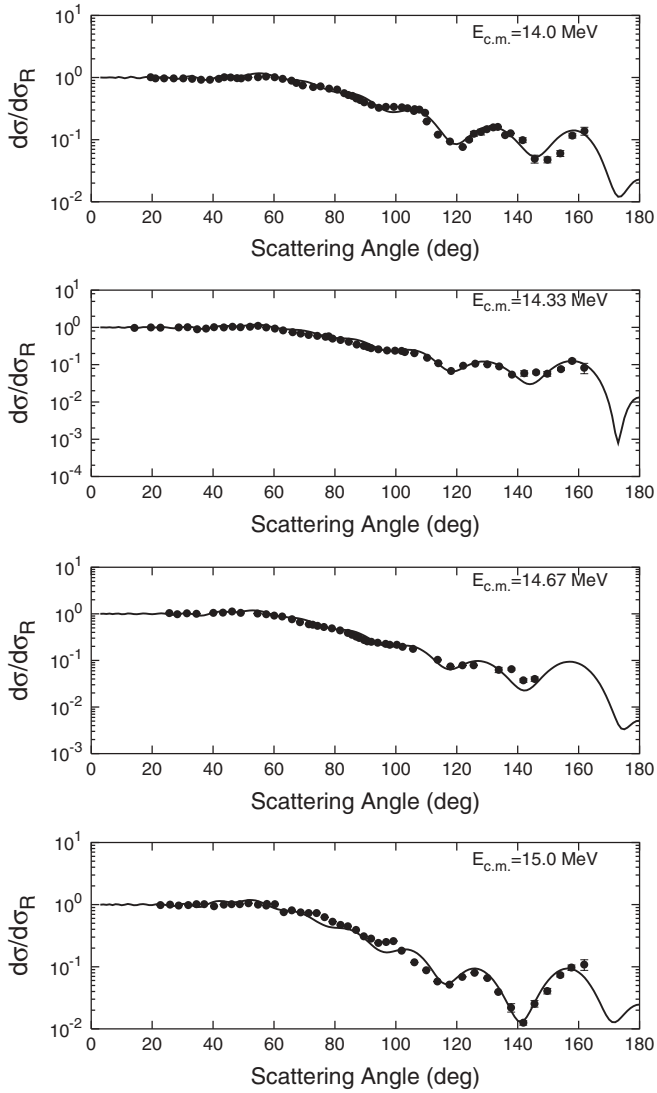

FIG. 12. Angular variation of elastic scattering cross section of $^{12}C+^{24}Mg$. The calculated results are shown by solid curve. The experimental values are shown by solid dots obtained from Ref. [6].

scattering cross section is given by

$$\frac{d\sigma}{d\sigma_R} = \left| \frac{f(\theta)}{f_C(\theta)} \right|^2. \tag{7}$$

III. CALCULATIONS FOR $^{16}O+^{28}SI$

For the $^{16}O+^{28}Si$ system, a large amount of experimental results of differential scattering cross-section $d\sigma/d\sigma_R$ (ratio to Rutherford cross section) as a function of center-of-mass angle θ over a wide range are available for several incident energies $E_{\text{c.m.}}$. These are for energies $E_{\text{c.m.}} = 18.67$, 19.03, 19.50, 20.12, 20.83, 21.10, 21.56, 22.29, 22.70, 24.30, 26.20, 31.82, and 35.0 MeV in the angular range $\theta = 0^\circ$ to 180° and for $E_{\text{c.m.}} = 33.727$, 36.909, 42.0, 45.818, 51.545, and 90.681 MeV in the angular range $\theta = 0^\circ$ to 100°. Extensive optical model analysis of the $^{16}O+^{28}Si$ system has been done by Boztosun [5]. His optical potential has the following features: (i) Real part having radial behavior given by sum of Woods-Saxon and Woods-Saxon derivative term with a very large depth of about 700 MeV at $r = 0$. (ii) A somewhat uncommon form factor for the imaginary potential which is taken to be sum of Woods-Saxon and Woods-Saxon derivative terms. (iii) The introduction of the Woods-Saxon derivative term in the optical potential as mentioned above introduces a slight nontrivial behavior at $r = R_0$ which is found to be crucial for fitting the experimental data. In all, his optical potential has 16 parameters, including the Coulomb radius parameter r_C, and they also introduce some energy dependence in some of the parameters. Thus, the whole conventional phenomenological nuclear optical potential is modified drastically to fit the low-energy data with reasonable success.

While undertaking systematic study of $d\sigma/d\sigma_R$ for the $^{16}O+^{28}Si$ system, we first examine whether the LC potential [17], which reproduces remarkably well the large back angle oscillations at $E_{\text{c.m.}} = 35.0$ MeV or $E_{\text{lab}} = 55.0$ MeV [18],

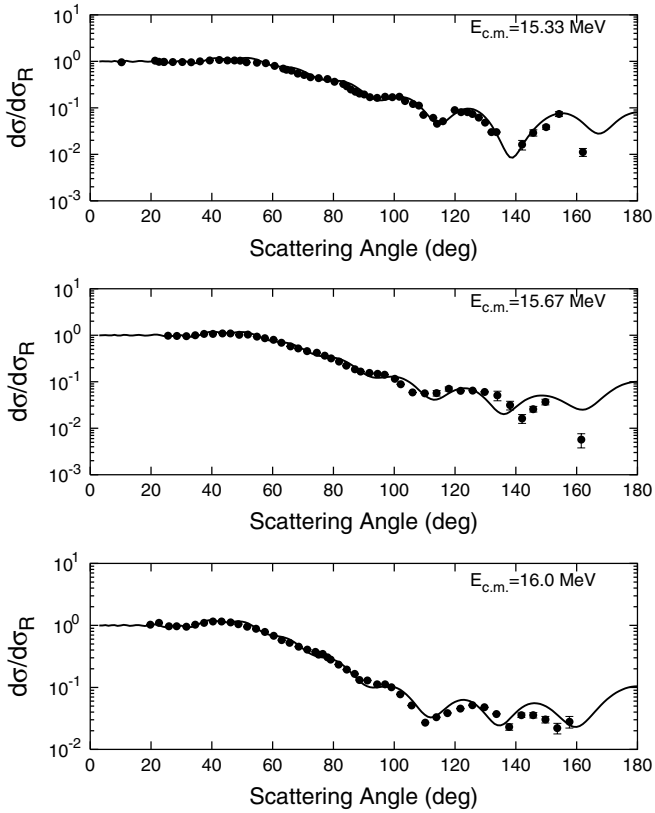

FIG. 13. Angular variation of elastic scattering cross section of $^{12}C+^{24}Mg$. The calculated results are shown by solid curve. The experimental values are shown by solid dots obtained from Ref. [6].

can be extended to wider energy range. This LC potential with seven parameters is given by

$$V_N(r) = (286.5 + i19.7)\left(1.0 + 0.99\exp\frac{r-R}{3.7} + \exp\frac{r-R}{0.49}\right)^{-1} \text{MeV}, \quad (8)$$

where $R = 1.122(A_P^{1/3} + A_T^{1/3})$. Using this potential, we carry out calculations of $d\sigma/d\sigma_R$ at a number of laboratory energies, namely $E_{\text{Lab}} = 50.0, 53.0, 55.0, 66.0, 72.0, 81.0$, and 142.5 MeV or $E_{\text{c.m.}} = 31.82$, 33.727, 35.0, 42.0, 45.818, 51.545, and 90.681 MeV in the angular range 0° to 180°, and conclude that this potential is quite satisfactory in fitting the available data that are confined to the angular region $\theta = 0^\circ$ to 100° in the E_{Lab} range 50.0 to 142.5 MeV [19] or $E_{\text{c.m.}} = 31.81$ to 90.681 MeV. However, when we extend the calculations to lower energies, for $E_{\text{c.m.}} = 18.67$ to 26.2 MeV experimental data of $d\sigma/d\sigma_R$ could not be fitted satisfactorily. In light of this and noting the importance of slight nontrivial behavior of optical potential in the Boztosun calculations, we decide to construct a new single optical potential for the entire energy range $E_{\text{c.m.}} = 18.67$ to 90.681 MeV using Ginocchio potential term as already described in Sec. II. To fit the $d\sigma/d\sigma_R$ data of the $^{16}O+^{28}Si$ system in the energy range from $E_{\text{c.m.}} = 18.67$ MeV to 26.20 MeV, we use Eq. (2) in the optical potential code we developed. Looking to the various effects

TABLE I. The parameters of $V_N(r)$ required to fit the lower-energy data of $^{16}O+^{28}Si$ are as follows: $R_0 = 8.5$ fm, $V_B = 2.35$ MeV, $B_0 = 26.0$, $R_{0W} = 9.25$ fm, $W_0 = 1.1$, $W_1 = 0.5$, and $W_2 = 0.18$. We have used $V_B = 1.8$ MeV at energy $E_{\text{c.m.}} = 26.20$ MeV for better fitting of the data. The parameters B_1, B_2, and V_{BW} of $V_N(r)$ are varied with the incident energies. These are given in this table.

$E_{\text{c.m.}}$ (MeV)	B_1	B_2	V_{BW} (MeV)	$E_{\text{c.m.}}$ (MeV)	B_1	B_2	V_{BW} (MeV)
18.67	0.5	0.55	0.058	21.56	1.38	0.16	0.18
19.03	0.6	0.53	0.058	22.29	1.5	0.16	0.18
19.50	0.67	0.5	0.058	22.70	1.7	0.16	0.18
20.12	0.82	0.4	0.135	24.30	2.0	0.16	0.18
20.83	1.00	0.35	0.135	26.20	2.05	0.05	0.38
21.10	1.1	0.3	0.135				

of the parameters on the potential, we vary the values of the parameters one after another during the fitting process. These values are found to be $R_0 = 8.5$ fm, $V_B = 2.45$ MeV, $B_0 = 26$ MeV, $R_{0W} = 9.25$ fm, $W_0 = 1.1$, $W_1 = 0.5$, and $W_2 = 0.18$. In the remaining three parameters B_1, B_2, and V_{BW}, we introduce some energy dependence as shown in Table I. When energy increases from 18.67 to 26.20 MeV, the value of B_1 increases from 0.5 to 2.05 and B_2 decreases from 0.55 to 0.05. As per the property of the parameters B_1 and B_2 mentioned in the formulation, the increase of B_1 makes the potential $V_1(r)$ to fall slowly in the interior side ($r < R_0$) and the decrease of B_2 takes the potential $V_2(r)$ to zero value sharply in the outer side ($r > R_0$). This can be clearly visualized in Fig. 2(a) where we plot the real potential at two energies: (i) the solid curve for energy $E_{\text{c.m.}} = 19.03$ MeV with $B_1 = 0.6$ and $B_2 = 0.53$ and (ii) the dashed curve with $B_1 = 2.05$ and $B_2 = 0.05$ for energy $E_{\text{c.m.}} = 26.20$ MeV.

Further, in Fig. 2(b), we plot the imaginary potential $W_n(r)$ with $V_{BW} = 0.058$ for energy $E_{\text{c.m.}} = 19.03$ MeV by a solid curve and compare the same with results shown by dashed line corresponding to $V_{BW} = 0.38$ for energy $E_{\text{c.m.}} = 26.20$ MeV. As expected, in addition to increasing the depth of the potential at $r = R_{0W}$, the increase in the value of V_{BW} increases the value of the slope parameter b_n on either side of $r = R_{0W}$ to make the potential vary sharply but uniformly. The change in the potentials at one energy to other seen in Fig. 2(b) is the total change for the whole energy range from 19.03 to 26.20 MeV.

Thus, in all we have 10 parameters for analysis of the data in this range as compared to 15 parameters used in Ref. [5]. In Figs. 3–5 we show the results of $d\sigma/d\sigma_R$ obtained by our calculations (full curves) along with the corresponding experimental data (solid dots). We find that our results fit the data in the entire angular range well and this can be considered remarkable because of the use of small number of parameters and wide energy range. Next, we extend the optical model calculations for this system for higher energies from 31.82 to 90.681 MeV where in most cases large angle data is not reported in literature except for 31.82 and 35.0 MeV. We find that in this energy range we can fit the experimental data using the parameters shown in Table II. It may be noted

TABLE II. The parameters of $V_N(r)$ required to fit the higher-energy data of $^{16}O+^{28}Si$ are as follows: $R_0 = 8.5$ fm, $V_B = 1.8$ MeV, $B_0 = 26.0$, $B_1 = 2.5$, $B_2 = 0.05$, $R_{0W} = 9.25$ fm, and $W_1 = 0.5$ The parameters V_{BW}, W_0, and W_2 of $V_N(r)$ are varied with the incident energies. These are given in this table.

$E_{c.m.}$ (MeV)	V_{BW} (MeV)	W_0	W_2	$E_{c.m.}$ (MeV)	V_{BW} (MeV)	W_0	W_2
31.82	0.9	1.5	0.18	42.0	1.8	2.4	0.5
33.727	0.9	2.0	0.25	45.818	2.1	3.0	0.75
35.00	1.4	2.0	0.27	51.545	2.2	3.4	0.95
36.909	1.4	2.0	0.27	90.681	2.2	5.0	1.3

that in this energy range we do not have to use the small energy dependence for parameters B_1 and B_2. However, the parameters V_{BW}, W_0, and W_2 of $V_N(r)$ are varied with the incident energies as shown in Table II to fit the data. We successfully explain the large angle oscillations in $d\sigma/d\sigma_R$ at energies $E_{c.m.} = 31.82$ and 35.0 MeV that are shown in Fig. 6. The results of our calculations for all other higher energies are shown in Figs. 7 and 8. Comparison of our results with experimental data indicates a quite good fit of the cross sections.

A very crucial test of the optical model analysis in HIC is the fitting of excitation function as a function of energy. In Fig. 9, we show the variation of excitation function as a function of energy obtained using our optical potential. It is remarkable that the large number of oscillations found in the excitation function data (solid dots) is fitted satisfactorily by our calculated results shown by a full curve.

Thus, based on the successful analysis of the results of $d\sigma/d\sigma_R$ at low energies in the angular range 0° to 180°, at higher energies in the angular range 0° to 100° and the excitation function in the center-of-mass energy range 13.0 to 52.0 MeV and comparison with earlier work of Boztosun, we conclude that introduction of slight nontrivial behavior in the surface region of real part of the optical potential is the most critical input and our potential incorporates this input using significantly lesser number of parameters.

IV. CALCULATIONS FOR $^{12}C+^{24}MG$

The $^{12}C+^{24}Mg$ system is another interesting case of HIC that has been studied recently by Sciani *et al.* [6] and Boztosun *et al.* [14] in the energy range $E_{c.m.} = 10.67$ to 16.0 MeV in the whole angular range $\theta = 0^\circ$ to 180°. Sciani has used a seven-parameter optical potential with Woods-Saxon form factor but failed to satisfactorily reproduce the oscillating angular distributions and for that reason the whole amount of data were analyzed simultaneously with the energy-dependent optical potential that gave somewhat more satisfactory fit in general. Even then, for the energy $E_{c.m.} = 14.0$ MeV, the fit in experimental data was not very satisfactory. In the calculations reported in Ref. [14], the optical potential used is similar to the one constructed for the $^{16}O+^{28}Si$ system [5] with a large number of parameters as discussed in the last section. Their results are satisfactory in the energy range $E_{c.m.} = 10.67$ to 16.0 MeV. In the light of the above and in view of the good results by us for the $^{16}O+^{28}Si$ system using our new optical potential, we extend our analysis to the $^{12}C+^{24}Mg$ system. In Table III, we list the potential parameters used in these calculations. As can be seen from the above Table III, the optical potential used by us has total of nine parameters, namely V_B, B_0, B_1, B_2, W_0, W_1, W_2, V_{BW}, and $R_0 = R_{0W}$. Of these, V_B, B_0, B_1, W_0, W_1, and W_2 are kept independent of energy, but R_0, V_{BW}, and B_2 are slightly varied with energy to obtain best fit to the experimental data.

TABLE III. The fixed parameters of nuclear potential required for best fit of elastic scattering cross sections of $^{12}C+^{24}Mg$ are as follows: $V_B = 2.6$ MeV, $B_0 = 17.6$, $B_1 = 0.45$, $W_0 = 2.0$, $W_1 = 0.2$, and $W_2 = 0.001$. The values of energy-dependent parameters for different $E_{c.m.}$ are given in this table.

$E_{c.m.}$ (MeV)	R_0 (fm)	B_2	V_{BW} (MeV)	$E_{c.m.}$ (MeV)	R_0 (fm)	B_2	V_{BW} (MeV)
10.67	8.32	0.24	0.005	14.00	7.90	0.40	0.045
11.33	8.29	0.27	0.0095	14.33	7.85	0.45	0.055
12.00	8.16	0.30	0.019	14.67	7.80	0.47	0.085
12.33	8.00	0.30	0.032	15.00	7.75	0.45	0.085
12.67	8.18	0.28	0.025	15.33	7.72	0.50	0.09
13.00	8.10	0.37	0.045	15.67	7.70	0.55	0.17
13.33	8.00	0.40	0.045	16.00	7.66	0.61	0.22
13.67	7.955	0.40	0.045				

In Figs. 10–13, we compare our calculated results shown by solid lines with the corresponding experimental results [6] shown by dots at several energies. It is clear from the results and their comparisons with results obtained by Sciani *et al.* [6] and Boztosun *et al.* [14] that the present Ginocchio-type optical potential is able to fit the data remarkably well.

V. DISCUSSION AND CONCLUSIONS

Now we discuss the critical features of the Ginocchio-type new optical potential, which is quite successful in fitting experimental data for the $^{16}O+^{28}Si$ and $^{12}C+^{24}Mg$ systems studied in this article. In fitting such data, it is necessary for the optical potential to generate partial-wave amplitudes with the correct magnitude and phase so that the oscillations observed in the data are accounted for. This optical model analysis for elastic scattering is fully a quantal formalism based on the one-body Schroedinger equation for the relative motion of the two colliding nuclei. The many-body aspects of the interaction are globally represented by average complex potential depending mainly on the relative coordinate. In our representation of the nuclear force, it is visualized that the nature of the nucleus-nucleus force in the interior (volume) region differs from that in the outer (surface) region though it is attractive in both the situations. Keeping this in view, we construct the nuclear potential by using Ginocchio-type expression that results in a nontrivial behavior in the surface region of the potential. This behavior affects the incoming wave packet containing large number of partial waves, each of which is experiencing phase shift $\delta(\ell)$. Superposition of these waves results in large-scale interference not fully

destructive but to provide an oscillatory result to account for the corresponding experimental angular distribution of the differential scattering cross section as well as excitation function.

It may be mentioned here that, in heavy-ion collisions, within the framework of semiclassical approximation, it is visualized that when the absorption is moderate in the interior region of the potential, the partial-wave amplitude can be written as a sum of an amplitude η_B describing a wave reflected at the barrier and an amplitude η_I corresponding to waves that penetrate into the interior region of the interaction potential [20,21]. With reference to grazing partial wave $\ell = \ell_g$ for a given incident energy, the amplitude η_B called the outer region amplitude is dominant at small angles, in other words, at large $\ell > \ell_g$ and the inner amplitude η_I is dominant at small $\ell < \ell_g$. The oscillation observed in the experimental scattering cross-section data can be understood as the result of interference between η_B and η_I. However, the estimate of these components requires further approximation such as strong absorption in the interior side for the calculation of η_B. The need for such a decomposition of scattering amplitude is avoided in our quantal calculation as outlined above.

In conclusion, we state that the new optical potential constructed using Ginocchio potential form has versatile features that gives a liberty to appropriately control surface and volume part of the interaction and nontrivial behavior in this surface region when necessary. This together with suitable energy dependence of some of the parameters is able to fit the $d\sigma/d\sigma_R$ data for the $^{16}O+^{28}Si$ system in the center-of-mass energy range 18.67 to 90.681 MeV and in the case of $^{12}C+^{24}Mg$ from a center-of-mass energy range of 10.67 to 16.0 MeV. This is achieved using substantially fewer parameters as compared to that used in other calculations reported in the literature. The critical role of the nontrivial behavior in the potential in the surface region is found to be important in generating the appropriate phase shift for each partial wave such that the superposition of large number of partial waves results in large-scale interference that consequently produces correct oscillation in differential scattering cross section and excitation function.

ACKNOWLEDGMENTS

We thank P. Prema for help in the preparation of the manuscript. This work is supported by the Board of Research in Nuclear Sciences (BRNS), Mumbai, India under Research Grant No. 2000/37/11/BRNS/704.

[1] M. C. Mermaz, E. R. Chavez-Lomeli, J. Barrette, B. Berthier, and A. Greiner, Phys. Rev. C **29**, 147 (1984).
[2] A. M. Kobos and G. R. Satchler, Nucl. Phys. **A427**, 589 (1984).
[3] D. Dehnhard, V. Shkolnik, and M. A. Franey, Phys. Rev. Lett. **40**, 1549 (1978).
[4] C. S. Shastry and I. Parija, Phys. Rev. C **27**, 2042 (1983).
[5] I. Boztosun, Phys. Rev. C **66**, 024610 (2002).
[6] W. Sciani *et al.*, Nucl. Phys. **A620**, 91 (1997).
[7] R. H. Siemssen, H. T. Fortune, R. Malmin, A. Richter, Y. W. Tippie, and P. P. Singh, Phys. Rev. Lett. **25**, 536 (1970).
[8] R. H. Siemssen, H. T. Fortune, A. Richter, and Y. W. Tippie, Phys. Rev. C **5**, 1839 (1972).
[9] V. Shkolnik, D. Dehnhard, and M. A. Franey, Phys. Rev. C **28**, 717 (1983).
[10] C. M. Cheng, J. V. Maher, W. Oelert, and F. D. Snyder, Phys. Lett. **B70**, 304 (1977).
[11] J. V. Maher, M. W. Sachs, R. H. Siemssen, A. Weidinger, and D. A. Bromley, Phys. Rev. **188**, 1665 (1969).
[12] W. Reilly, R. Wieland, A. Gobbi, M. W. Sachs, and D. A. Bromley, Nuovo Cimento A **13**, 897 (1973).
[13] W. Reilly, R. Wieland, A. Gobbi, M. W. Sachs, J. Maher, R. H. Siemssen, D. Mingay, and D. A. Bromley, Nuovo Cimento A **13**, 913 (1973).
[14] I. Boztosun and W. D. M. Rae, Phys. lett. **B518**, 229 (2001).
[15] J. N. Ginocchio, Ann. Phys. **152**, 203 (1984).
[16] B. Sahu, G. S. Mallick, and S. K. Agarwalla, Nucl. Phys. **A727**, 299 (2003).
[17] S. Y. Lee and Y. D. Chan, preprint, University of Washington, 1978.
[18] T. Takemasa and T. Tamura, Phys. Rev. C **18**, 1282 (1978).
[19] S. K. Agarwalla, G. S. Mallick, P. Prema, S. Mahadevan, B. Sahu, and C. S. Shastry, J. Phys. G: Nucl. Part. Phys. **32**, 165 (2006).
[20] D. M. Brink and Takigawa, Nucl. Phys. **A279**, 159 (1977).
[21] D. M. Brink, *Semi-Classical Methods for Nucleus-Nucleus Scattering* (Cambridge University Press, Cambridge, UK, 1985).
[22] J. G. Cramer, R. M. DeVries, D. A. Goldberg, M. S. Zisman, and C. F. Maguire, Phys. Rev. C **14**, 2158 (1976).